

Robust topological superconductivity in spin-orbit coupled systems at higher-order van Hove filling

Xinloong Han,^{1,*} Jun Zhan,^{2,3,†} Fu-chun Zhang,¹ Jiangping Hu,^{2,1,‡} and Xianxin Wu^{4,§}

¹*Kavli Institute for Theoretical Sciences, University of Chinese Academy of Sciences, Beijing 100190, China*

²*Beijing National Laboratory for Condensed Matter Physics and Institute of Physics, Chinese Academy of Sciences, Beijing 100190, China*

³*School of Physical Sciences, University of Chinese Academy of Sciences, Beijing 100190, China*

⁴*CAS Key Laboratory of Theoretical Physics, Institute of Theoretical Physics, Chinese Academy of Sciences, Beijing 100190, China*

(Dated: February 10, 2023)

Van Hove singularities (VHSs) in proximity to the Fermi level promote electronic interactions and generate diverse competing instabilities. It is also known that a nontrivial Berry phase derived from spin-orbit coupling (SOC) can introduce an intriguing decoration into the interactions and thus alter correlated phenomena. However, it is unclear how and what type of new physics can emerge in a system featured by the interplay between VHSs and the Berry phase. Here, based on a general Rashba model on the square lattice, we comprehensively explore such an interplay and its significant influence on the competing electronic instabilities by performing a parquet renormalization group analysis. Despite the existence of a variety of comparable fluctuations in the particle-particle and particle-hole channels associated with higher-order VHSs, we find that the chiral $p \pm ip$ pairings emerge as two stable fixed trajectories within the generic interaction parameter space, namely the system becomes a robust topological superconductor. The chiral pairings stem from the hopping interaction induced by the nontrivial Berry phase. The possible experimental realization and implications are discussed. Our work sheds new light on the correlated states in quantum materials with strong SOC and offers fresh insights into the exploration of topological superconductivity.

Introduction.—Topological superconductivity has been attracting tremendous attention owing to the potential use in topological quantum computation of the hosted Majorana modes [1, 2]. As the intrinsic topological superconductivity usually necessitates an exotic p -wave pairing, which is rare in nature, major experimental efforts focus on realizing synthetic p -wave states through exploiting the superconducting proximity effect in heterostructures [3–9], including nanowire-superconductor and topological-insulator-superconductor setups. In both cases, spin-orbit coupling, generating band splittings or topological surface states, plays an indispensable role in the synthetic pairing but has no direct interplay with electronic interactions.

In two-dimensional (2D) hetero-structures, interfaces and moiré materials, fascinating correlated phenomena often emerge [10–18], such as superconductivity. The ubiquitous SOC, whose strength can be tuned by external electric fields [19, 20], is capable of significantly modifying the electronic properties [21, 22]. Apart from that, another essential feature of SOC is that it introduces an intriguing Berry curvature field on the single-particle wavefunctions and thus a nontrivial geometric phase in the reciprocal space, which can dramatically alter interaction-driven phenomena [23–25]. On the other hand, van Hove (VH) singularities in the vicinity of Fermi energy in 2D materials, exhibiting divergent density of states (DOS), can generate diverse competing correlated states [26–32]. For conventional VH singularities (VHSs), they feature logarithmically divergent DOS and particle-particle instability is usually dominant unless

there is perfectly nested Fermi surface [27–30]. In contrast, higher-order VHSs are characterized by stronger power-law divergent DOS and the corresponding fluctuations in particle-particle and particle-hole channels are comparable [31–35], resulting stronger competition. Once SOC is introduced in the VH dispersion, often occurring in 2D quantum materials, the concomitant band splitting lifts spin degeneracy and saddle points, moving away from high-symmetry momentum points, acquire a nontrivial Berry phase. They tend to put strong constraint on the electronic interactions and modify the competing instabilities. Therefore, it is desirable to explore the delicate interplay between electronic correlations associated with VHSs and geometric phases derived from SOC [25].

In this Letter, we present a comprehensive study about the interplay between higher-order VHSs and the nontrivial Berry phase through a weak-coupling renormalization group analysis. The non-interacting Hamiltonian is based on a general Rashba model on the square lattice, where higher-order VHSs are realized. Based on the simplified patch model, the parquet renormalization group calculations are adopted for two representative higher-order van Hove dispersion. We find that chiral $p \pm ip$ pairings emerge as two stable fixed trajectories in the interaction parameter space and are dominant with generic interaction setting, demonstrating a robust topological superconductivity. This chiral pairing is intimately correlated with a pair hopping interaction involving a nontrivial Berry phase and the corresponding transition temperature is expected to be high. An interacting super-

metal phase with power-law divergent density of states but no long-range order [32] can be stabilized at some parameter regime. The possible experimental realization and implications are also discussed.

Model and effective Theory.— We start with a generic tight-binding model with nearest-neighbor (NN) Rashba SOC terms on a square lattice,

$$\mathcal{H}_{\text{TB}} = - \sum_{\langle i,j \rangle_{n\sigma}} t_n (c_{i\sigma}^\dagger c_{j\sigma} + \text{h.c.}) - \mu_0 \sum_{i\sigma} n_{i\sigma} + \frac{i}{2} \lambda_R \sum_{(ij),\sigma,\sigma'} c_{i\sigma}^\dagger (\boldsymbol{\sigma}_{\sigma\sigma'} \times \mathbf{d}_{ij})_z c_{j\sigma'}, \quad (1)$$

where $c_{i\sigma}$ is the electron annihilation operator on the lattice site i with a spin projection $\sigma = \uparrow, \downarrow$, t_n is the hopping parameter between the n -th NN sites and λ_R is the Rashba SOC constant between the NN sites with \mathbf{d}_{ij} being the connecting vectors and $\boldsymbol{\sigma}$ being the Pauli matrices. Two conventional VHSs appear at the X points in the absence of SOC but they move along the X– Γ or X–M lines in two helicity space upon including SOC. For example, with hopping up to the next NN sites, the positive-helicity band $E_+(\mathbf{q})$ hosts a saddle point on the Γ –X line and it is located at $P^+ = (\pi - \arctan \frac{\lambda_R}{2t_1 + 4t_2}, 0)$. The corresponding low-energy dispersion expanded up to the quadratic terms reads $E_{P^+}(\mathbf{k}) = \mu_{\text{VH}} - D_1 k_x^2 + D_2 k_y^2$ where (k_x, k_y) is the deviation from the P^+ point, here $\mu_{\text{VH}} = -2t_1 + D_0$, $D_1 = D_0$ and $D_2 = t_1 + \frac{1}{2}D_0 - 4t_2(1 + 2t_2)/D_0$ with $D_0 = \frac{1}{2}\sqrt{\lambda_R^2 + 4(t_1 + 2t_2)^2}$. With further inclusion of longer-range hopping parameters, one coefficient of quadratic terms can vanish, realizing a higher-order VHS. In Fig.1(a), we display a representative tight-binding band dispersion with four higher-order VHSs in the vicinity of the Fermi level. Around the saddle point on the Γ –X line, the low-energy dispersion is $E(\mathbf{k}) = Ak_y^2 - Bk_x^4$ with constants $A, B > 0$ and it displays flat dispersion along the k_x direction (as shown in Fig.1(a) and (c)), contributing a power-law divergent density of states (DOS) $\nu(E) \propto |E|^{-\kappa}$ with an exponent $\kappa = 1/4$. As shown in Fig.1(b), the corresponding Fermi surface is endowed with an intricate spin texture and this introduces an intriguing geometric phase for the four VHSs, where the Fermi surface touches tangentially (black circles in Fig.1(c)). Other kinds of higher-order VHSs with distinct DOS exponents κ can also be realized in this model and details are given the supplementary material (SM) [36]. An interesting case is the VH dispersion with $E(\mathbf{k}) = Ak_x^3 - 3Bk_x k_y^2$ and $\kappa = 1/3$, where three Fermi surfaces touch at the saddle points.

We turn to study the correlation effect at the VH filling. Owing to the divergent DOS of VHSs, the collective electronic phenomena are expected to be dominated by the electronic scattering around these saddle points. Therefore, we can simplify the above non-interacting

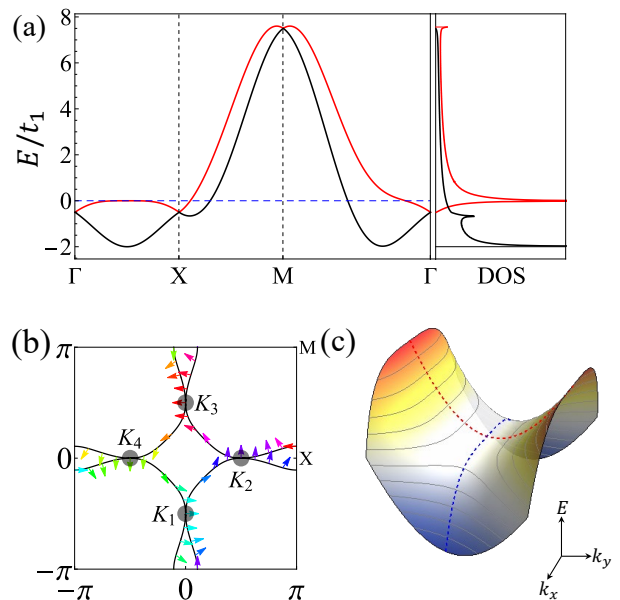


FIG. 1. (a) Energy dispersion of the two Rashba-split bands and their density of states. Four higher-order VHSs are located at the Fermi level (blue dashed line) and the adopted parameters are $\lambda_R = t_1, t_2 = -t_1/2, t_3 = -\lambda_R/8, \mu_0 = -t_1$. (b) Fermi surface of the positive-helicity band hosting higher-order VHSs and its spin texture. (c) 2D dispersion around the higher-order saddle point with $E(\mathbf{k}) = A(-k_x^4 + k_y^2)$

Hamiltonian and come to a low-energy patch model,

$$\mathcal{H}_0 = \sum_{\alpha=1}^4 \sum_{|\mathbf{k}| < k_\Lambda} \hat{c}_{\alpha\mathbf{k}}^\dagger [\epsilon_\alpha(\mathbf{k}) - \mu] c_{\alpha\mathbf{k}}, \quad (2)$$

where \mathbf{k} is centred at the saddle point $\alpha = K_i$ ($i = 1, 2, 3, 4$), as illustrated in the Fig. 2(a), with a patch size k_Λ associated with the ultraviolet energy cutoff Λ . The $\epsilon_\alpha(\mathbf{k})$ is the general low-energy dispersion around the higher-order saddle point α . The non trivial spin texture of these VHSs is analogous to putting a monopole at the center of the Brillouin zone, as shown in Fig.2(a). The nesting property and exponent κ in the DOS are related to the VH dispersion and several kinds of higher-order VHSs have been discussed and realized in various platforms [31–34, 37]. Our following treatment works for general VHSs and we choose two typical higher-order VH dispersion to show the essential characteristics: (a) $\epsilon_{K_1}^e(\mathbf{k}) = A(k_x^2 - k_y^4)$ and two Fermi surface touch tangentially at the saddle point [31, 32], (b) $\epsilon_{K_1}^o(\mathbf{k}) = A(k_y^3 - 3k_x k_y^2)$ and three Fermi surfaces touch at the saddle point [33]. The dispersion around other patches can be obtained $\epsilon_{K_i}(\mathbf{k}) = \epsilon_{K_1}(\hat{C}_4^{i-1}\mathbf{k})$ with \hat{C}_4 being the $\pi/2$ clockwise rotation operation.

Within this patch model, we consider all possible electron-electron interactions between the patches and

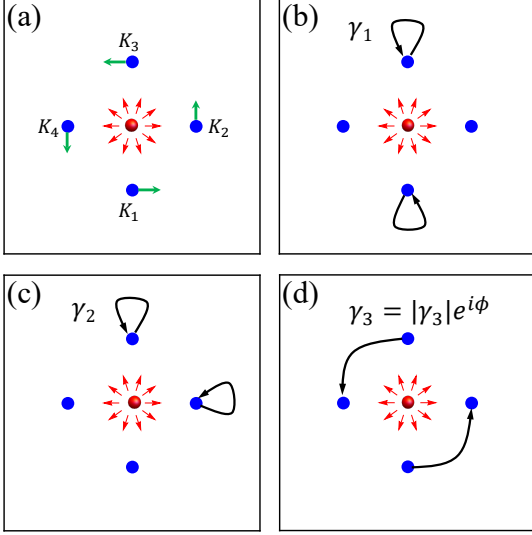


FIG. 2. (a) Low-energy patch model on the square lattice. The green arrow denotes the spin texture in each patch from the Dirac monopole (red sphere) at the center. (b,c,d) Three allowed interactions from the momentum conservation and fermionic nature and the pairing hopping process (γ_3) obtains a nontrivial Berry phase.

only three interactions are allowed[28, 29, 38, 39],

$$\begin{aligned} \mathcal{H}_{\text{int}} = & \frac{1}{2N} \sum_{\alpha=1}^4 \sum'_{|\mathbf{k}_1|, \dots, |\mathbf{k}_4| < k_\Lambda} \left[\gamma_1 c_{\bar{\alpha}\mathbf{k}_1}^\dagger c_{\alpha\mathbf{k}_2}^\dagger c_{\alpha\mathbf{k}_3} c_{\bar{\alpha}\mathbf{k}_4} + \right. \\ & \gamma_2 c_{\langle\alpha\rangle\mathbf{k}_1}^\dagger c_{\alpha\mathbf{k}_2}^\dagger c_{\alpha\mathbf{k}_3} c_{\langle\alpha\rangle\mathbf{k}_4} + (|\gamma_3| e^{i\phi} c_{\bar{\alpha}+1\mathbf{k}_1}^\dagger c_{\alpha+1\mathbf{k}_2}^\dagger c_{\bar{\alpha}\mathbf{k}_3} \\ & \left. \times c_{\alpha\mathbf{k}_4} + h.c. \right], \end{aligned} \quad (3)$$

where $\sum'_{|\mathbf{k}_1|, \dots, |\mathbf{k}_4| < k_\Lambda} = \sum_{|\mathbf{k}_1|, \dots, |\mathbf{k}_4| < k_\Lambda} \delta_{\mathbf{k}_1+\mathbf{k}_2, \mathbf{k}_3+\mathbf{k}_4}$ and N is the number of unit cells. The patch $\langle\alpha\rangle$ and $\bar{\alpha}$ denotes the NN and the opposite patches of the patch α , respectively. As shown in Fig.2(b)-(d), γ_1 and γ_2 are the density-density interactions between opposite patches and NN patches while γ_3 is the pair hopping interaction. Remarkably, due to the presence of a Dirac monopole, this pair hopping process will accumulate a nontrivial Berry phase as $e^{i\phi}$ with $\phi \in [-\pi, \pi]$ [23–25, 40]. In the tetragonal systems, this phase is fixed to $\phi = \pm\frac{\pi}{2}$, determined by the corresponding charge of the monopole $c = \pm 1$. In contrast to the hexagonal systems [25], $\phi = 0$ is not allowed in our case but corresponds to a vanishing γ_3 due to the lattice rotational symmetry and fermionic nature. This nontrivial Berry phase, as shown in the following, plays a pivotal role in determining the leading instability.

Susceptibilities and RG equations.— Next, we perform renormalization group analysis to unveil competing electronic instabilities. Before deriving the RG equations, we first analyse particle-particle (pp) and particle-hole (ph) susceptibilities to determine which kinds of

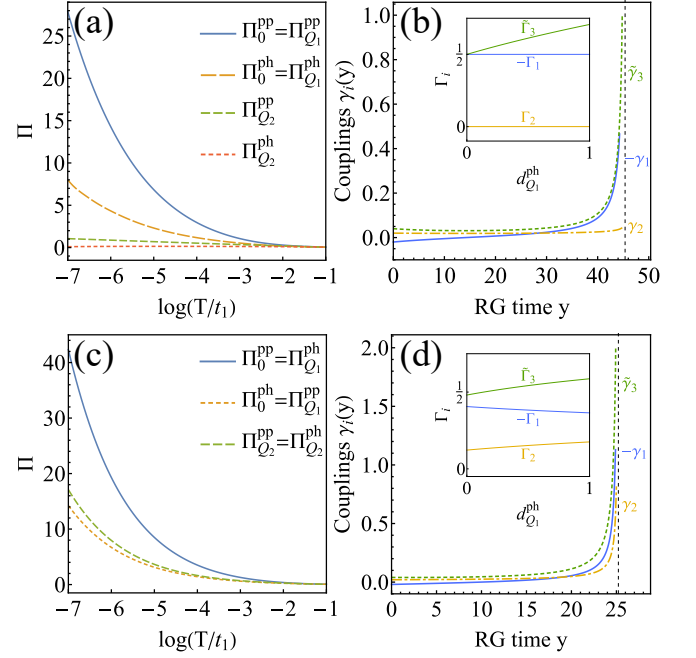


FIG. 3. Susceptibilities (a,c) as functions of $\log(T/t_1)$ and RG flows (b,d) with initial repulsive interaction $\gamma_{1,2}(0) = 0.02$ and $\tilde{\gamma}_3(0) = 0.04$. Inset figures show the critical interactions Γ_i as functions of $d_{\mathbf{Q}_1}^{\text{ph}}$ with $\tilde{\Gamma}_3 = -i\Gamma_3$. The upper and bottom panels denote the cases of the higher-order VH dispersion with $\epsilon_\alpha^e(\mathbf{k})$ and $\epsilon_\alpha^o(\mathbf{k})$, respectively.

scattering channels are relevant near the Fermi energy. The static susceptibilities are defined as $\Pi_{\mathbf{Q}}^{\text{pp/ph}} = \pm T \sum_n \int_{\mathbf{k}} G(\mathbf{k}, \omega_n) G(\mp\mathbf{k} + \mathbf{Q}, \mp\omega_n)$. Here $G(\mathbf{k}, \omega_n) = 1/(i\omega_n - \xi_{\alpha,\mathbf{k}})$ is the bare Green's function of electrons with energy $\xi_{\alpha,\mathbf{k}} = \epsilon_\alpha(\mathbf{k}) - \mu$ and fermionic Matsubara frequency $\omega_n = (2n+1)\pi T$. We focus on the VH filling $\mu = 0$ and asymptotic limit $\Lambda \gg T$. The particle-particle and particle-hole susceptibilities with zero momentum transfer in the patch model acquire the leading power-law divergence $\Pi_0^{\text{pp}} = \frac{1}{\kappa} \Pi_0^{\text{ph}} = C_0 T^{-\kappa}$. Two relevant momentum transfer are between opposite patches $\mathbf{Q}_1 = 2\mathbf{Q}_\alpha$ and NN patches $\mathbf{Q}_2 = \mathbf{K}_\alpha - \mathbf{K}_{\alpha+1}$. While, behaviours of susceptibilities at \mathbf{Q}_1 and \mathbf{Q}_2 strongly depend on the dispersion around the saddle point. By adopting numerical calculations, we plot all particle-particle and particle-hole susceptibilities for $\epsilon_\alpha^e(\mathbf{k})$ and $\epsilon_\alpha^o(\mathbf{k})$ as a function of the temperature in the Fig.3 (a) and (c), respectively. In the former case, susceptibilities with \mathbf{Q}_1 in both channels are power-law divergent due to $\epsilon_\alpha^e(\mathbf{k}) = \epsilon_\alpha^e(-\mathbf{k})$ and others with \mathbf{Q}_2 are constant or logarithmically divergent thus negligible. In the latter case, however, all susceptibilities with \mathbf{Q}_1 and \mathbf{Q}_2 are comparable and $\Pi_{\mathbf{Q}_1}^{\text{ph/pp}} = \Pi_0^{\text{pp/ph}}$ due to $\epsilon_\alpha^o(\mathbf{k}) = -\epsilon_\alpha^o(-\mathbf{k})$. To quantify the relative susceptibilities with respect to the Cooper instability, we introduce the nesting parameter,

$$d_{\mathbf{q}}^{\text{pp/ph}} = \lim_{T/\Lambda \rightarrow 0} \frac{\partial \Pi_{\mathbf{q}}^{\text{pp/ph}}(T)}{\partial \Pi_0^{\text{pp}}(T)}. \quad (4)$$

Here a non-zero $d_{\mathbf{q}}^{\text{pp/ph}}$ represents a relevant susceptibility $\Pi_{\mathbf{q}}^{\text{pp/ph}}$. For the $\epsilon_{\alpha}^e(\mathbf{k})$, $d_{\mathbf{0}}^{\text{pp}} = d_{\mathbf{Q}_1}^{\text{pp}} = 1$, $d_{\mathbf{0}}^{\text{ph}} = d_{\mathbf{Q}_1}^{\text{ph}} = 1/4$, $d_{\mathbf{Q}_2}^{\text{pp}} = d_{\mathbf{Q}_2}^{\text{ph}} = 0$. For the $\epsilon_{\alpha}^o(\mathbf{k})$, $d_{\mathbf{0}}^{\text{pp}} = d_{\mathbf{Q}_1}^{\text{pp}} = 1$, $d_{\mathbf{0}}^{\text{ph}} = d_{\mathbf{Q}_1}^{\text{ph}} = 1/3$, $d_{\mathbf{Q}_2}^{\text{pp}} = d_{\mathbf{Q}_2}^{\text{ph}} \simeq 0.39$. The details of calculations are given in the SM. The determination of these parameters for a general higher-order VH dispersion needs numerical calculations but the essential feature is that fluctuations in multiple pp and ph channels are comparable, in contrast to the conventional VHS [25, 30].

By using the dominant susceptibilities as building blocks, we can derive RG equations for the dimensionless interactions $\tilde{\gamma}_i = \gamma_i \partial \Pi_{\mathbf{0}}^{\text{pp}} / \partial s$ including both tree-level and one-loop terms with the RG time $s = \ln(\Lambda/T)$. We find that all corresponding fixed points are generally unstable (see SM) and thus we focus on their strong-coupling trajectories, where certain interactions diverge towards a critical RG time. In this case, the tree-level terms are irrelevant and we can conveniently simplify the RG equations for the dimensional interactions [34, 35],

$$\begin{aligned} \partial_y \gamma_1 &= (d_{\mathbf{Q}_1}^{\text{ph}} - 1)\gamma_1^2 - 2d_{\mathbf{0}}^{\text{ph}}\gamma_2^2 - |\gamma_3|^2, \\ \partial_y \gamma_2 &= (d_{\mathbf{Q}_2}^{\text{ph}} - d_{\mathbf{Q}_2}^{\text{pp}})\gamma_2^2 - 2d_{\mathbf{0}}^{\text{ph}}\gamma_1\gamma_2 + d_{\mathbf{Q}_2}^{\text{ph}}|\gamma_3|^2, \\ \partial_y \gamma_3 &= -2d_{\mathbf{0}}^{\text{pp}}\gamma_1\gamma_3 + 4d_{\mathbf{Q}_2}^{\text{ph}}\gamma_2\gamma_3, \end{aligned} \quad (5)$$

where we change the RG time to $y = \Pi_{\mathbf{0}}^{\text{pp}}(T) - \Pi_{\mathbf{0}}^{\text{pp}}(\Lambda)$. As γ_1 and γ_2 terms conserves the number of electrons at each patch separately but γ_3 does not, the β function of γ_3 must contain an overall factor of itself. Further considering the absence of γ_3^* terms in the β function, the associated phase of γ_3 remains fixed during the RG evolution. Since the β function for γ_1 becomes negative definite, i.e. $\partial_y \gamma_1 < 0$, γ_1 always tends to flow negative infinity from a negative initial value, promoting instabilities in both pp and ph channels.

To determine the possible competing instabilities, we introduce the test vertices in various pp and ph channels, $\delta \mathcal{H}_I = \sum_{\alpha\alpha'} [\Delta_{\alpha\alpha'}^I c_{\alpha}^{\dagger} c_{\alpha'}^{(\dagger)} + h.c.]$. Under the RG flow, they obtain one-loop corrections through the divergent susceptibilities, $\partial_y \Delta^I = -d^I \mathcal{M}^I \Delta^I$ with $d^I = d_{\mathbf{q}}^{\text{pp/ph}}$ and \mathcal{M}^I being the corresponding driving interaction matrix. These orders can be further decoupled into different irreducible channels according to the lattice symmetry. Approaching the critical RG time y_c , interactions diverge and usually flow into some fixed trajectories, which can be parameterized as $\gamma_i(y) = \Gamma_i/(y_c - y)$. Hence, the vertices will diverge as $\Delta_I(y) \propto (y_c - y)^{\eta_I}$ and the corresponding susceptibility scales as $\chi_I \propto (y_c - y)^{2\eta_I+1}$, implying that only vertices with $\eta_I < -1/2$ are relevant instabilities and the order with most negative η_I is the leading instability. We list all possible orders in various channels and the corresponding exponents in the Table I (for details see SM). The lifted spin degeneracy imposes strong constraints on the instabilities. In the

TABLE I. Divergent exponents η_I for all competing orders in the pp and ph channels.

particle-particle order	particle-hole order
$\eta_{p \pm ip}^{\text{SC}} = 2d_{\mathbf{0}}^{\text{pp}}(\Gamma_1 \mp \tilde{\Gamma}_3)$	$\eta_s^{\text{Pom}} = 2d_{\mathbf{0}}^{\text{ph}}(\Gamma_1 \pm 2\Gamma_2)$
	$\eta_p^{\text{Pom}} = -2d_{\mathbf{0}}^{\text{ph}}\Gamma_1$
	$\eta_{\mathbf{Q}_1}^{\text{CDW}} = -2d_{\mathbf{Q}_1}^{\text{ph}}\Gamma_1$
$\eta_{\mathbf{Q}_2}^{\text{PDW}} = 2d_{\mathbf{Q}_2}^{\text{pp}}\Gamma_2$	$\eta_{\mathbf{Q}_2, \pm}^{\text{CDW}} = 2d_{\mathbf{Q}_2}^{\text{ph}}(-\Gamma_2 \pm \tilde{\Gamma}_3)$

particle-particle channel, the intra-patch pairing density wave (PDW) is forbidden and only the p -wave pairing between the opposite patches is allowed. The $p + ip$ and $p - ip$ pairing states get split owing to the pair hopping scattering γ_3 involving a Berry phase.

Competing instabilities.— We first study the characteristic flow with initial repulsive interactions. With defining $\tilde{\gamma}_3 = -i\gamma_3$, we plot the RG flows of the coupling constants from starting repulsive interactions as $\gamma_{1,2}(0) = 0.02$ and $\gamma_3(0) = 0.04i$ for higher-order VH fillings with $\epsilon_{\alpha}^e(\mathbf{k})$ and $\epsilon_{\alpha}^o(\mathbf{k})$ in the Fig.3 (b) and (d), respectively. All interactions diverge approaching a critical RG time and the critical value in the latter case is smaller due to the additional boost of $\Pi_{\mathbf{Q}_2}^{\text{pp/ph}}$ related terms. These interactions flow into one fixed trajectory and the evolution of Γ_i as function of $d_{\mathbf{q}}^{\text{ph}}$ are displayed in the insets. We find that Γ_2 is zero for $\epsilon_{\alpha}^e(\mathbf{k})$, indicating that γ_2 diverges slower than $1/(y_c - y)$. For $\epsilon_{\alpha}^o(\mathbf{k})$, all three interactions are comparable. In this fixed trajectory, the dominant instability is the $p_x + ip_y$ pairing according to Table I. To determine all fixed trajectories and their stability[29, 41, 42], we introduce the following reduced RG equations for the relative interactions $x_i = \gamma_i/\gamma_1$ ($i = 2, 3$) with RG time proxy γ_1 ,

$$\begin{aligned} \frac{dx_2}{d \ln |\gamma_1|} &= \frac{(d_{\mathbf{Q}_2}^{\text{ph}} - d_{\mathbf{Q}_2}^{\text{pp}})x_2^2 - 2d_{\mathbf{0}}^{\text{ph}}x_2 + d_{\mathbf{Q}_2}^{\text{ph}}|x_3|^2}{d_{\mathbf{Q}_1}^{\text{ph}} - d_{\mathbf{0}}^{\text{pp}} - 2d_{\mathbf{0}}^{\text{ph}}x_2^2 - d_{\mathbf{0}}^{\text{pp}}|x_3|^2} - x_2, \\ \frac{dx_3}{d \ln |\gamma_1|} &= \frac{-2d_{\mathbf{Q}_1}^{\text{pp}}x_3 + 4d_{\mathbf{Q}_2}^{\text{ph}}x_2x_3}{d_{\mathbf{Q}_1}^{\text{ph}} - d_{\mathbf{0}}^{\text{pp}} - 2d_{\mathbf{0}}^{\text{ph}}x_2^2 - d_{\mathbf{0}}^{\text{pp}}|x_3|^2} - x_3. \end{aligned} \quad (6)$$

The nontrivial fixed trajectories (Γ_i) of Eq. (5) then will have a correspondence with the fixed points in Eq.(6) as $(\Gamma_2/\Gamma_1, \Gamma_3/\Gamma_1)$. In the Fig. 4(a),(b), we illustrate the RG flow diagrams of ratios $x_{2,3}$ for higher-order VHSs with $\epsilon_{\alpha}^e(\mathbf{k})$ and $\epsilon_{\alpha}^o(\mathbf{k})$. The common feature in both cases is that there are two stable fixed points at the positive and negative finite $\tilde{\gamma}_3/\gamma_1$ values, corresponding to the chiral $p_x \mp ip_y$ superconducting states (red point-up/point-down triangle). In contrast to the only two nontrivial fixed points for $\epsilon_{\alpha}^e(\mathbf{k})$, there are four more fixed points for the $\epsilon_{\alpha}^o(\mathbf{k})$. Three of them are unstable, corresponding to the d -wave Pomeranchuk order (blue hexagon) and additional chiral $p \pm ip$ pairing (blue triangles), and the rest one is stable (red square), which is a degenerate point for the $p \pm ip$ pairing and s-wave charge Pomeranchuk or-

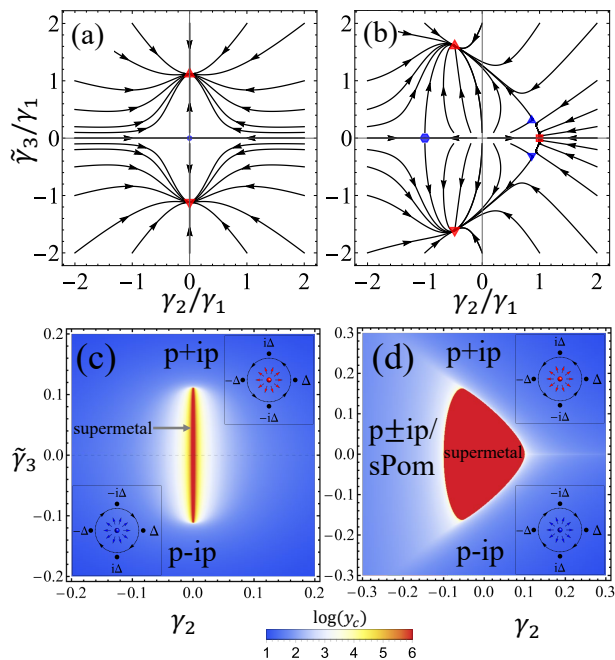


FIG. 4. RG flow diagrams of the reduced RG equation Eq. 6 in the parameter space $(\gamma_2/\gamma_1, \tilde{\gamma}_3/\gamma_1)$ for the $\epsilon_\alpha^e(\mathbf{k})$ (a) and $\epsilon_\alpha^o(\mathbf{k})$ (b), with $\gamma_1 < 0$. Phase diagrams for the higher-order VHSs with $\epsilon_\alpha^e(\mathbf{k})$ (c) and $\epsilon_\alpha^o(\mathbf{k})$ (d) for the initial interaction $\gamma_1(0) = 0.1$. The color map represents the critical RG scale $\log(y_c)$ and the red region, namely too large y_c , denotes that there is no instability.

der (sPom). The degeneracy and stability are related to the dispersion and these states can be split once κ deviates from $\frac{1}{3}$. We further display the phase diagrams for general initial interactions in Fig. 4(c),(d). It is apparent that the chiral superconductivity dominates the phase diagram in both cases. An interacting supermetal phase, exhibiting divergent DOS and finite dimensionless interaction but no long-range order [32], emerges on certain line for $\epsilon_\alpha^e(\mathbf{k})$ and certain region for $\epsilon_\alpha^o(\mathbf{k})$ and there is a strong CDW fluctuation in the latter case (see SM). The three-fold degenerate state, corresponding to the fixed point (red square) in Fig. 4(b), can appear for an initial strong attractive γ_2 .

Despite comparable fluctuations in the multiple pp and ph channels at the higher-order VH filling, we find robust instability in the pp channel with zero momentum, determined by the negative definite interaction γ_1 . The pair hopping scattering γ_3 involving a nontrivial Berry phase further promotes a chiral pairing, corresponding to a mixture between equal-spin and spin-singlet pairing due to the broken inversion symmetry. Owing to the power-law divergent DOS, the superconducting transition temperature scales as $T_c \propto \lambda^{1/\kappa}$ with λ being coupling constant, compared with the case of conventional VHS $T_c \propto e^{-1/\lambda}$. In the realistic systems, several kinds of higher-order VHSs has been realized in stoichiometric materials, het-

erostructures and twisted systems [31, 37, 43–46]. The crucial factor is to introduce an additional SOC and this can be achieved in inversion-breaking materials with heavy atom substitution. In heterostructures and moiré materials SOC can be further enhanced and tuned by the external electric field [45–47]. Once higher-order VHSs with SOC are realized, the electric gating approach can be used to introduce carrier doping and tune electronic instabilities. An important feature of chiral superconductivity is that it can host Majorana zero modes in the vortex, which can be detected using experimental technique, such as scanning tunneling microscope [48].

Conclusions and remarks.— In summary, we show that the interplay of higher-order VHSs and a nontrivial Berry phase has a dramatic impact on the competing electronic instabilities within the RG formalism. The chiral $p \pm ip$ pairings, directly related to the pair hopping process involving a Berry phase, emerge as two stable fixed trajectories in the interaction parameter space and are dominant in the phase diagram with generic interaction setting. The supermetal phase can appear in certain parameter regime and an s -wave Pomeranchuk order in degenerate with $p \pm ip$ pairing states can be stabilized for a strong initial attractive γ_2 for the case of $\kappa = \frac{1}{3}$. Our work demonstrates the robust chiral superconductivity in spin-orbit coupled systems at higher-order VH filling and offers fresh insights into the exploration of topological superconductivity.

Acknowledgments.— We acknowledge the supports by the Ministry of Science and Technology (Grant No. 2022YFA1403901), National Natural Science Foundation of China (No. 11920101005, No. 11888101) and the New Cornerstone Investigator Program. F.C.Z is also partially supported by the Priority Program of Chinese Academy of Sciences (Grant No. XDB28000000). X.L.H also acknowledges the supports from China Postdoctoral Science Foundation Fellowship (No. 2022M723112).

* hanxinloong@gmail.com; These authors equally contributed to the work.

† These authors equally contributed to the work.

‡ jphu@iphy.ac.cn

§ xxwu@itp.ac.cn

- [1] M. Z. Hasan and C. L. Kane, *Rev. Mod. Phys.* **82**, 3045 (2010).
- [2] X.-L. Qi and S.-C. Zhang, *Rev. Mod. Phys.* **83**, 1057 (2011).
- [3] R. M. Lutchyn, E. P. A. M. Bakkers, L. P. Kouwenhoven, P. Krogstrup, C. M. Marcus, and Y. Oreg, *Nature Reviews Materials* **3**, 52 (2018).
- [4] Y. Oreg, G. Refael, and F. von Oppen, *Phys. Rev. Lett.* **105**, 177002 (2010).
- [5] R. M. Lutchyn, J. D. Sau, and S. Das Sarma, *Phys. Rev. Lett.* **105**, 077001 (2010).
- [6] J. D. Sau, R. M. Lutchyn, S. Tewari, and S. Das Sarma,

- Phys. Rev. Lett.* **104**, 040502 (2010).
- [7] M. T. Deng, S. Vaitiekėnas, E. B. Hansen, J. Danon, M. Leijnse, K. Flensberg, J. Nygård, P. Krogstrup, and C. M. Marcus, *Science* **354**, 1557 (2016).
- [8] L. Fu and C. L. Kane, *Phys. Rev. Lett.* **100**, 096407 (2008).
- [9] M.-X. Wang, C. Liu, J.-P. Xu, F. Yang, L. Miao, M.-Y. Yao, C. L. Gao, C. Shen, X. Ma, X. Chen, Z.-A. Xu, Y. Liu, S.-C. Zhang, D. Qian, J.-F. Jia, and Q.-K. Xue, *Science* **336**, 52 (2012).
- [10] N. Reyren, S. Thiel, A. D. Caviglia, L. F. Kourkoutis, G. Hammerl, C. Richter, C. W. Schneider, T. Kopp, A.-S. Rüetschi, D. Jaccard, M. Gabay, D. A. Muller, J.-M. Triscone, and J. Mannhart, *Science* **317**, 1196 (2007).
- [11] A. Gozar, G. Logvenov, L. F. Kourkoutis, A. T. Bollinger, L. A. Giannuzzi, D. A. Muller, and I. Bozovic, *Nature* **455**, 782 (2008).
- [12] C. Liu, X. Yan, D. Jin, Y. Ma, H.-W. Hsiao, Y. Lin, T. M. Bretz-Sullivan, X. Zhou, J. Pearson, B. Fisher, J. S. Jiang, W. Han, J.-M. Zuo, J. Wen, D. D. Fong, J. Sun, H. Zhou, and A. Bhattacharya, *Science* **371**, 716 (2021).
- [13] S. Qin, J. Kim, Q. Niu, and C.-K. Shih, *Science* **324**, 1314 (2009).
- [14] T. Zhang, P. Cheng, W.-J. Li, Y.-J. Sun, G. Wang, X.-G. Zhu, K. He, L. Wang, X. Ma, X. Chen, Y. Wang, Y. Liu, H.-Q. Lin, J.-F. Jia, and Q.-K. Xue, *Nature Physics* **6**, 104 (2010).
- [15] Y. Cao, V. Fatemi, A. Demir, S. Fang, S. L. Tomarken, J. Y. Luo, J. D. Sanchez-Yamagishi, K. Watanabe, T. Taniguchi, E. Kaxiras, R. C. Ashoori, and P. Jarillo-Herrero, *Nature* **556**, 80 (2018).
- [16] Y. Cao, V. Fatemi, S. Fang, K. Watanabe, T. Taniguchi, E. Kaxiras, and P. Jarillo-Herrero, *Nature* **556**, 43 (2018).
- [17] Y. Tang, L. Li, T. Li, Y. Xu, S. Liu, K. Barmak, K. Watanabe, T. Taniguchi, A. H. MacDonald, J. Shan, and K. F. Mak, *Nature* **579**, 353 (2020).
- [18] E. C. Regan, D. Wang, C. Jin, M. I. Bakti Utama, B. Gao, X. Wei, S. Zhao, W. Zhao, Z. Zhang, K. Yumigeta, M. Blei, J. D. Carlström, K. Watanabe, T. Taniguchi, S. Tongay, M. Crommie, A. Zettl, and F. Wang, *Nature* **579**, 359 (2020).
- [19] J. Nitta, T. Akazaki, H. Takayanagi, and T. Enoki, *Phys. Rev. Lett.* **78**, 1335 (1997).
- [20] J. B. Miller, D. M. Zumbühl, C. M. Marcus, Y. B. Lyanda-Geller, D. Goldhaber-Gordon, K. Campman, and A. C. Gossard, *Phys. Rev. Lett.* **90**, 076807 (2003).
- [21] A. D. Caviglia, M. Gabay, S. Gariglio, N. Reyren, C. Cancellieri, and J.-M. Triscone, *Phys. Rev. Lett.* **104**, 126803 (2010).
- [22] G. Herranz, G. Singh, N. Bergeal, A. Jouan, J. Lesueur, J. Gázquez, M. Varela, M. Scigaj, N. Dix, F. Sánchez, and J. Fontcuberta, *Nature Communications* **6**, 6028 (2015).
- [23] J. Shi and Q. Niu, *Science China Physics, Mechanics & Astronomy* **63**, 227422 (2019).
- [24] L. Mao, J. Shi, Q. Niu, and C. Zhang, *Phys. Rev. Lett.* **106**, 157003 (2011).
- [25] W. Qin, L. Li, and Z. Zhang, *Nature Physics* **15**, 796 (2019).
- [26] L. Van Hove, *Phys. Rev.* **89**, 1189 (1953).
- [27] H. J. Schulz, *Europhysics Letters* **4**, 609 (1987).
- [28] N. Furukawa, T. M. Rice, and M. Salmhofer, *Phys. Rev. Lett.* **81**, 3195 (1998).
- [29] R. Nandkishore, L. S. Levitov, and A. V. Chubukov, *Nature Physics* **8**, 158 (2012).
- [30] H. Yao and F. Yang, *Phys. Rev. B* **92**, 035132 (2015).
- [31] N. F. Q. Yuan, H. Isobe, and L. Fu, *Nature Communications* **10**, 5769 (2019).
- [32] H. Isobe and L. Fu, *Phys. Rev. Res.* **1**, 033206 (2019).
- [33] A. Shtyk, G. Goldstein, and C. Chamon, *Phys. Rev. B* **95**, 035137 (2017).
- [34] L. Classen, A. V. Chubukov, C. Honerkamp, and M. M. Scherer, *Phys. Rev. B* **102**, 125141 (2020).
- [35] Y.-P. Lin and R. M. Nandkishore, *Phys. Rev. B* **102**, 245122 (2020).
- [36] See Supplemental Material at *** for details on the tight-binding model, susceptibilities and RG analysis for dimensionless interactions..
- [37] D. V. Efremov, A. Shtyk, A. W. Rost, C. Chamon, A. P. Mackenzie, and J. J. Betouras, *Phys. Rev. Lett.* **123**, 207202 (2019).
- [38] K. L. Hur and T. Maurice Rice, *Annals of Physics* **324**, 1452 (2009), July 2009 Special Issue.
- [39] W. Metzner, M. Salmhofer, C. Honerkamp, V. Meden, and K. Schönhammer, *Rev. Mod. Phys.* **84**, 299 (2012).
- [40] C. Zhang, S. Tewari, R. M. Lutchyn, and S. Das Sarma, *Phys. Rev. Lett.* **101**, 160401 (2008).
- [41] I. Herbut, *A Modern Approach to Critical Phenomena* (Cambridge University Press, 2007).
- [42] O. Vafek and K. Yang, *Phys. Rev. B* **81**, 041401 (2010).
- [43] R. S. Markiewicz, B. Singh, C. Lane, and A. Bansil, arXiv e-prints, arXiv:2105.04546 (2021), arXiv:2105.04546 [cond-mat.str-el].
- [44] D. Di Sante, X. Wu, M. Fink, W. Hanke, and R. Thomale, *Phys. Rev. B* **99**, 201106 (2019).
- [45] Z. Bi and L. Fu, *Nature Communications* **12**, 642 (2021).
- [46] D. Guerzi, P. Simon, and C. Mora, *Phys. Rev. Res.* **4**, L012013 (2022).
- [47] H. Pan, F. Wu, and S. Das Sarma, *Phys. Rev. Res.* **2**, 033087 (2020).
- [48] D. Wang, L. Kong, P. Fan, H. Chen, S. Zhu, W. Liu, L. Cao, Y. Sun, S. Du, J. Schneeloch, R. Zhong, G. Gu, L. Fu, H. Ding, and H.-J. Gao, *Science* **362**, 333 (2018).